Journal of Modern Optics

ISSN: 0950-0340 (Print) 1362-3044 (Online) Journal homepage: http://www.tandfonline.com/loi/tmop20

# The transition from a coherent optical vortex to a Rankine vortex: beam contrast dependence on topological charge

**Ermes Toninelli, Reuben S. Aspden, David Phillips, Graham M. Gibson & Miles J. Padgett**

**To cite this article:** Ermes Toninelli, Reuben S. Aspden, David Phillips, Graham M. Gibson & Miles J. Padgett (2016) The transition from a coherent optical vortex to a Rankine vortex: beam contrast dependence on topological charge, Journal of Modern Optics, 63:sup3, S51-S56, DOI: 10.1080/09500340.2016.1234651

**To link to this article:** http://dx.doi.org/10.1080/09500340.2016.1234651



Published online: 21 Sep 2016.

JOURNAL OF MODERN OPTICS, 2016
VOL. 63, NO. S3, S51–S56
http://dx.doi.org/10.1080/09500340.2016.1234651

Taylor & Francis
Taylor & Francis Group



# The transition from a coherent optical vortex to a Rankine vortex: beam contrast dependence on topological charge

Ermes Toninelli, Reuben S. Aspden, David Phillips, Graham M. Gibson and Miles J. Padgett

School of Physics and Astronomy, University of Glasgow, Glasgow, UK

**ABSTRACT**

Spatially coherent helically phased light beams carry orbital angular momentum (OAM) and contain phase singularities at their centre. Destructive interference at the position of the phase singularity means the intensity at this point is necessarily zero, which results in a high contrast between the centre and the surrounding annular intensity distribution. Beams of reduced spatial coherence yet still carrying OAM have previously been referred to as Rankine vortices. Such beams no longer possess zero intensity at their centre, exhibiting a contrast that decreases as their spatial coherence is reduced. In this work, we study the contrast of a vortex beam as a function of its spatial coherence and topological charge. We show that beams carrying higher values of topological charge display a radial intensity contrast that is more resilient to a reduction in spatial coherence of the source.

**ARTICLE HISTORY**
Received 27 May 2016
Accepted 3 September 2016

**KEYWORDS**
Rankine vortex; spatial coherence; helically-phased beam; OAM; speckle; spatial coherence length; singularity; contrast

## 1. Introduction

Spatially coherent light beams containing phase singularities are used within optical physics, where their angular momentum and/or their annular intensity cross-section lead to interesting effects (*1*–*4*). Of particular prominence are those beams with helical phase-fronts described by a term $\exp(i\ell\phi)$, where $\phi$ is the azimuthal angle within the beam and $\ell$, the topological charge, is an integer describing the number of intertwined helical phase surfaces, i.e. the rotational symmetry of the complex field. These helically phased beams carry an orbital angular momentum (OAM) of $\ell\hbar$ per photon, in addition to the photons intrinsic spin angular momentum (*5*, *6*).

A common method for generating helically phased beams is to illuminate a diffraction grating containing a fork dislocation with a spatially coherent Gaussian beam thereby generating a vortex beam in the first diffraction order (*7*). A forked-diffraction grating of this type is effectively an off-axis hologram of a spiral phase plate formed from a glass disc with a thickness that increases with azimuthal angle, such that a plane-wave, when transmitted through the plate, acquires helical phase-fronts. The hologram grating to be displayed on a spatial light modulator (SLM) to modulate the phase of the first-order pattern is the following:

$$\Phi(x,y) = \left(\frac{2\pi}{\Lambda}x + \ell \arctan2\left(\frac{y}{x}\right)\right) \mathrm{mod} 2\pi, \qquad (1)$$

where $x$ and $y$ are the Cartesian coordinates from the centre of the incident beam on the SLM and $\Lambda$ is the grating period.

When using a light source of reduced spatial coherence, the contrast of the resulting optical vortex is also reduced. If one seeks to utilize the optical vortex it is usual to introduce a spatial filter prior to the vortex mask, such as to restrict the illumination source to a single transverse mode, albeit at the expense of optical throughput (*8*). In this work, we consider relaxing the degree of spatial filtering so that multiple transverse modes are transmitted. We study the trade-off between the observed contrast of the vortex centre and transmitted intensity as a function of the spatial coherence and the azimuthal index of the vortex filter.

Swartzlander *et al.* studied the action of a spiral phase plate when the spatial coherence of the illumination is reduced, resulting in a so-called 'Rankine' vortex rather than a coherent vortex beam (*8*). The term Rankine vortex first originated in fluid dynamics (*9*): a Rankine vortex-type flow-field possesses two regions of differing rotational character. Below a specific radius, viscous

**CONTACT** Ermes Toninelli e.toninelli.1@research.gla.ac.uk
Raw data can be found in the open-access repository at http://dx.doi.org/10.5525/gla.researchdata.315.

forces ensure there is no slippage between fluid layers, i.e. the entire region rotates like a solid object, and the tangential flow velocity is proportional to the radius $r$. At distances above this specific radius, viscous friction between fluid layers is overcome and slippage between the layers occurs. In this region, the tangential velocity is inversely proportional to $r$. An optical Rankine vortex is created by imparting a helical phase delay onto a beam of reduced spatial-coherence length (*10*). By considering illumination of reduced spatial-coherence as a lateral distribution of a multitude of sources, incoherent with respect to each other, one is able to describe the resulting Rankine vortex as the incoherent sum of many helically phased beams, slightly displaced with respect to the beam axis and indeed each other (*11*, *12*). Studies of partially coherent vortices have also been extended to consider their cross-correlation functions (*13*).

Analogously to the fluidic case, an optical Rankine vortex also exhibits two regions of differing character, in this case relating to the directional energy flux density (which can be described by the Poynting vector, $S$). For the case of a *spatially coherent* vortex beam, the azimuthal component of the Poynting vector is given by: $S_\varphi = (S_0\ell)/(k_0 r)$, where $k_0$ is the wavenumber $2\pi/\lambda$ and $r$ the radial distance from the centre of the vortex (i.e. proportional to $1/r$ ) (*14*). In contrast, an optical Rankine vortex exhibits a time-averaged expectation value for $S_\varphi$ that for small $r$ is proportional to $r$, whilst approximating to $1/r$ for large $r$ (i.e. the same as the purely coherent optical vortex case). It is therefore clear that Rankine vortices no longer exhibit a point of zero intensity on the beam axis, and so the contrast across its transverse intensity profile is reduced.

Beams containing Rankine vortices are relevant to applications of the OAM of light under conditions of turbulence or other time-varying aberrations (*15*), for example, optical communication, imaging and optical micromanipulation (*16*). We also note that the study of spiral phase filters, as applied to light of finite spatial coherence, is closely related to both spiral phase microscopy (*17*, *18*) and optical vortex coronagraphs (*19*).

In this work, we ask a simple question: '*How do the intensity contrast and transmitted power of a vortex beam vary for different values of $\ell$, as the degree of spatial filtering of a partially coherent source is changed?*'

## 2. Experiment

The experimental apparatus used in this present study is shown in Figure 1. Our partially spatially coherent source is a Schell-model source, consisting of a Gaussian spot of laser light focused on a continuously rotating ground-glass plate (RGP) and followed by a compound lens ($\times 5$ microscope objective) placed at its effective focal length away from the RGP (*20*). We use an adjustable aperture to control the degree of spatial filtering of our partially coherent source. More specifically, the output from a HeNe laser is focused onto the RGP (which acts as a diffuser) and the transmitted light is collimated and coupled into a step-index multi-mode optical fibre, with a core diameter of 50 $\mu$m. The output of this fibre is imaged onto an aperture, the size of which can be adjusted, so that one or more optical speckles are transmitted. The number of speckles transmitted by the aperture is related to the number of transverse modes in the transmitted light. The spatial filtering of the partially coherent output of the multi-mode fibre controls the degree of spatial coherence of the light. The light transmitted through this aperture is again re-collimated and used to illuminate an SLM, positioned in the far-field of the fibre facet and acting as a programmable diffractive optical element, suitable for implementing the forked-diffraction grating. Finally, a 16-bit dynamic-range camera (Camera 1, *HAMAMATSU, ORCA-flash4.0*) is positioned in the far-field of the SLM so that the resulting beam cross-section can be imaged and recorded. For ease of alignment and comparison to the spatially coherent case, the multi-mode fibre can be replaced with a single-mode fibre, yielding a high fidelity helically phased beam at Camera 1.

## 3. Results

In order to relate the contrast of our Rankine beams to the number of speckle grains transmitted through the system, we recorded two sets of data. The first set, shown in Figure 2, consisted of the images recorded by Camera 1. We used them to calculate the contrast, $C$, of the vortex beams, $C = (I_{\max} - I_{\min})/(I_{\max} + I_{\min})$, where $I_{\max}$ is the signal in the bright annular region and $I_{\min}$ is the intensity in the middle, dark regions. These images highlight the transition from a pure optical vortex (Figure 2(a), (d) and (g)) to a Rankine vortex for three increasing values of $\ell$. Figure 2(b), (e) and (h) correspond to a $\approx$ 50% reduction in contrast, whereas Figure 2(c), (f) and (i) correspond to the lowest measured contrast.

The second set of data was acquired from an 8-bit dynamic-range camera (Camera 2, *TELEDYNE, DALSA Genie*). We used these images for two purposes: (1) Estimating the average size of a speckle grain and (2) Measuring the size of the aperture. We defined the spatial coherence length (SCL) as the Gaussian full width at half maximum of the autocorrelated speckle-patterns, averaged over a large number of patterns. The average size of a grain (i.e. the SCL) was obtained by computing the autocorrelation of hundreds of speckle patterns,

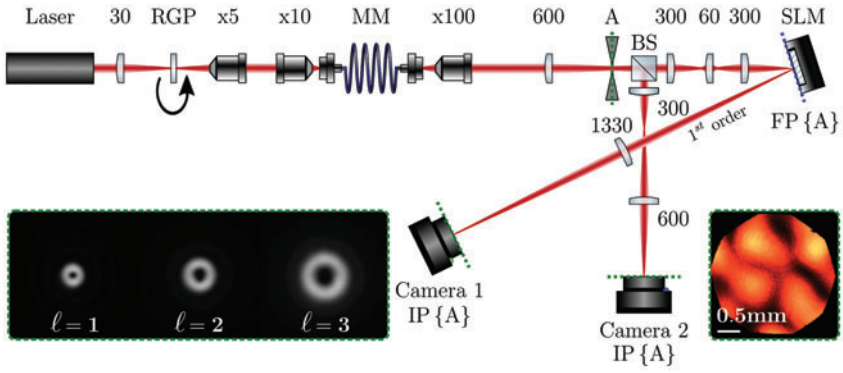


**Figure 1. Experimental apparatus.** A HeNe laser is focused on a rotating ground glass plate (RGP) by a 30 mm lens and coupled into a multi-mode fibre using ×5 and ×10 microscope objectives. A ×100 microscope objective and a 600 mm lens are used to reimage the output facet of the fibre onto a varying aperture (A). This beam is demagnified using 300 mm and 60 mm lenses. A 300 mm lens collimates the beam on the SLM, which is placed in the Fourier plane (FP) of the aperture. A further 1330 mm lens collects the 1st diffraction order from the SLM and images the aperture on to Camera 1, which is itself in the FP of the SLM. The inset on the left shows the OAM pattern for different $\ell$ values for the single-mode case, as recorded by Camera 1, whereas the inset on the right shows a stationary speckle pattern on the plane of the aperture, as recorded by Camera 2.

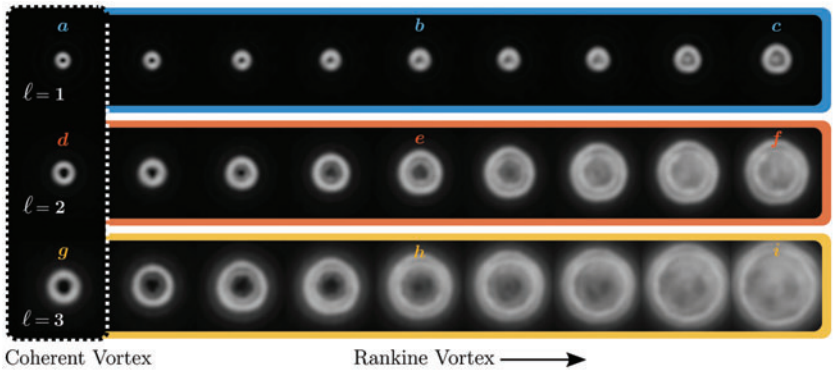


**Figure 2. The transition from a pure optical vortex to a Rankine vortex.** The intensity patterns at Camera 1 are shown for different $\ell$ values, in the transition from a pure optical vortex (as shown in (a), (d) and (g)) to a Rankine vortex. A $\approx$ 50% contrast reduction was found for (b), (e) and (h), whereas (c), (f) and (i) correspond to the lowest measured contrast.

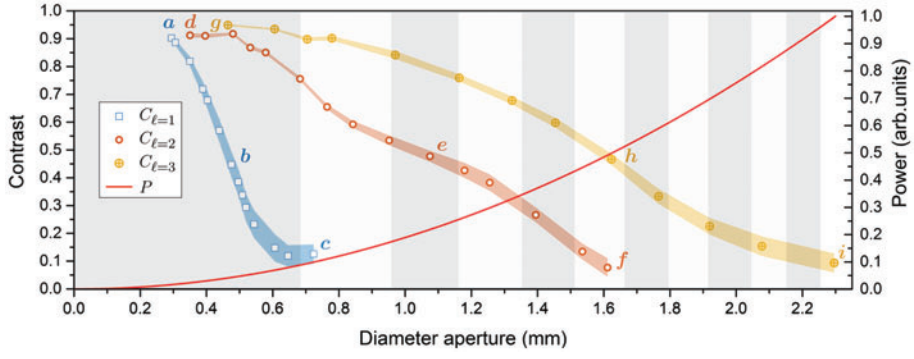


**Figure 3. Beam contrast as a function of the degree of spatial filtering (i.e. aperture diameter) of the partially coherent source for different spiral-phase masks.** The graph shows the beam contrast as a function of the aperture diameter for different values of $\ell$ and an estimate of power (red solid line). The alternating grey and white vertical bands represent the degree of spatial filtering in terms of the number of transmitted speckle grains through the aperture. The contrast between the central dark and the bright annular regions is shown to decrease as the diameter of the aperture is increased. As expected the transmitted power increases with the diameter of the aperture.

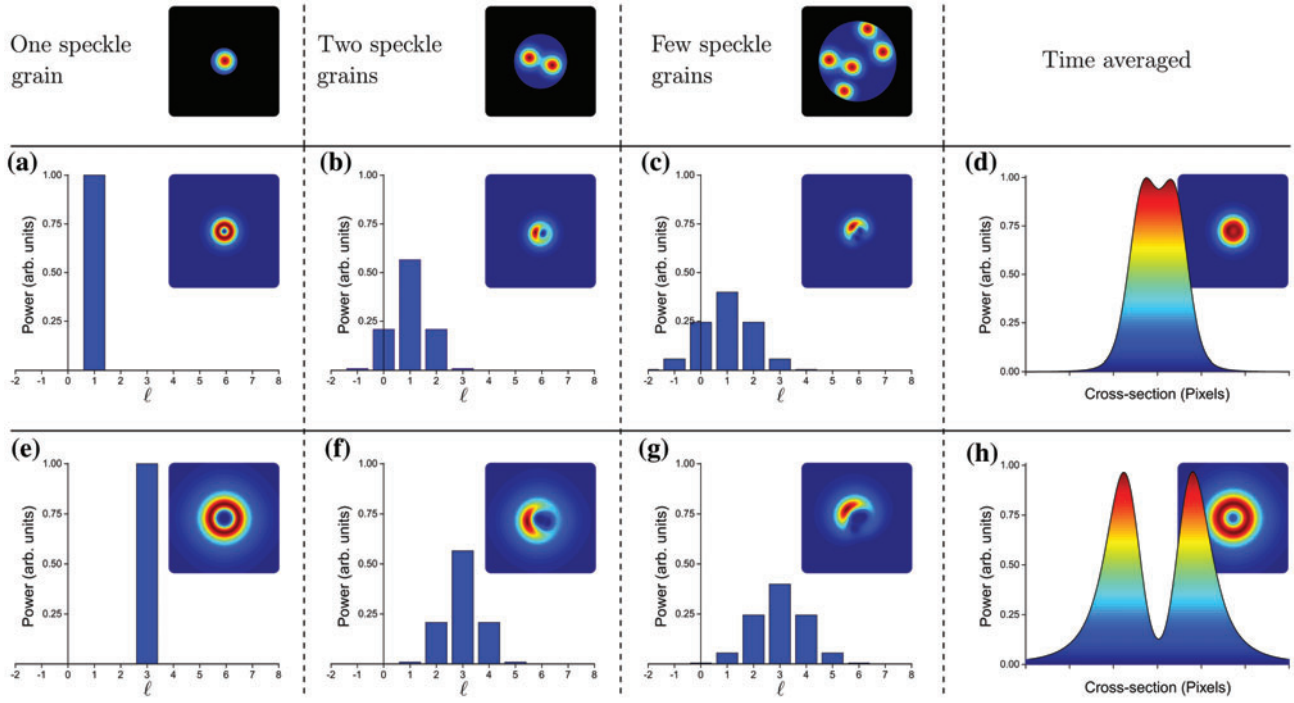


**Figure 4. Representation of the power decomposition for $\ell = 1$ and $\ell = 3$ OAM modes.** (a)-(c) shows a schematic of OAM modal decomposition for $\ell = 1$ for progressively decreasing spatial coherence. (d) shows the intensity profile of a simulated example of a Rankine vortex for $\ell = 1$. (e)–(g) shows a schematic of OAM modal decomposition for $\ell = 3$ for progressively decreasing spatial coherence. (h) shows the intensity profile of a simulated example of a Rankine vortex for $\ell = 3$.

recorded by Camera 2. For this purpose, the RGP was used as a stationary diffuser, producing patterns like the one shown in the right inset of Figure 1. The SCL for our system was calculated to be $0.68\,\text{mm} \pm 0.07\,\text{mm}$. We used this value to estimate the degree of spatial filtering of the partially coherent source, in terms of the number of transmitted speckle grains for different aperture sizes and $\ell$ values. These findings are summarized in Figure 3. An indicator of the degree of spatial filtering in multiples of SCL for a certain aperture diameter is given by the alternating grey and white vertical bands. The decrease in contrast is shown to vary suddenly for $C_{\ell=1}$ reaching a minimum for an aperture diameter corresponding to approximately one SCL. For $C_{\ell=2}$ and $C_{\ell=3}$, the contrast was found to be more resilient, resulting in a $\approx 50\%$ reduction, respectively, for three and six SCLs. Finally, the shaded error-bars for the contrast curves were calculated by taking into consideration the intensity discrepancies in the bright annular region as well as different intensities of the neighbouring pixels around the centre.

As one would expect, the transmitted power $P$, detected at Camera 1 was found to be proportional to the size of the aperture, increasing in a quadratic fashion. $P$ is plotted in red in Figure 3 for the reader's convenience. As it can be observed, a reduction in contrast is linked to an increase in transmitted power.

## 4. Discussion

The results show that the radial contrast of the beam is inversely related to the degree of spatial filtering introduced by the variable aperture, as the topological charge of the beam increases. Figure 4 is a schematic that explains the reasons behind this phenomenon. As the diameter of the aperture is reduced below the average speckle grain size, the output of the system tends to a coherent vortex (as shown in the first column of Figure 4). The OAM modal decomposition (also known as the OAM spectrum) describes the relative power in different OAM modes forming a beam. In the coherent case, all of the power in the beam is found in a single OAM mode, as shown schematically for $\ell = 1$ in Figure 4(a), and for $\ell = 3$ in Figure 4(e).

As the diameter of the aperture is increased, so too is the number of speckle grains that are transmitted through the aperture, effectively reducing the degree of spatial filtering. Each speckle grain can be considered as a coherent source with a randomized relative phase. Using this description, at the SLM plane each speckle grain approximates a plane-wave illuminating the SLM from a different angle. Each such plane-wave results in a coherent vortex beam at the camera, laterally displaced off-axis by a vector determined by the incident angle on

the SLM. When multiple speckle grains are present at one instant, they form laterally displaced OAM beams which interfere with one another at the plane of Camera 1. The OAM spectra of such a field exhibit a spread into the neighbouring OAM modes, as shown schematically for $\ell = 1$ in Figure 4(b), and for $\ell = 3$ in Figure 4(f). The fields shown in the inset of Figure 4(b) and (f) are simulations representing one member of an ensemble of interference patterns, which in our experiment can be observed when the RGP is stationary. Further increasing the size of the aperture decreases the amount of spatial filtering, allowing the transmission of more speckle grains and therefore exacerbates the spreading of the OAM decomposition. This is illustrated schematically in Figure 4(c) and (g).

When the RGP is rotating, Camera 1 measures the time-averaged intensity distribution of the ensemble. Temporal averaging causes the central region of the beam to have a non-zero intensity, when the aperture is larger than the average speckle grain size. At the centre of the Rankine vortex, the time-averaged azimuthal energy flow and momentum are proportional to $r$. In terms of radial contrast, any power diverted to the $\ell = 0$ mode of the time-averaged OAM spectra results in a non-zero on-axis intensity at the centre of the vortex, and consequently in a lower contrast value. For a given aperture diameter, more power is spread into the $\ell = 0$ mode for lower values of topological charge. This effect is depicted in Figure 4(b) and (f), where the $\ell = 1$ case exhibits more power diverted to the $\ell = 0$ mode than the $\ell = 3$ case. The last column of Figure 4 shows examples of simulated temporally incoherent sum of approximately five-hundred individual members of the ensemble, for $\ell = 1$ and $\ell = 3$. The intensity profiles of the resulting Rankine vortices are plotted in Figure 4(d) and (h).

## 5. Conclusions

We have investigated the transition from a purely helically phased beam to a Rankine vortex, as the degree of spatial coherence of the illumination was gradually decreased by allowing more speckle grains to propagate through the system. We have shown that for higher values of topological charge, the radial intensity contrast of a beam is more resilient to a reduction in spatial coherence of the source. This can be understood by considering the instantaneous OAM modal-decomposition of one member of the ensemble of light fields that form the beam (*21*, *22*). When an OAM beam is slightly displaced off-axis, power is spread into neighbouring modes of the OAM decomposition. Light can only be transferred to the central on-axis region of the beam if power is spread into the $\ell = 0$ mode (as all others have zero intensity at their centre). Therefore in the case of an averaged ensemble, beams of higher $\ell$ are found to spread less power into the $\ell = 0$ mode, for a given reduction of spatial coherence. We believe this effect to be relevant to light-starved applications, where one wishes to reduce the degree of spatial filtering required. Especially at high $\ell$-values, a significant increase in illumination flux is achievable with only a modest reduction in contrast. Such a trade-off may be applicable within low-light imaging applications in either classical (*17*) or quantum domains (*18*).

## Acknowledgements

We thank Miguel Angel Olvera Santamaria for fruitful discussions about spatial coherence of vortex beams.

## Disclosure statement

No potential conflict of interest was reported by the authors.

## Funding

ET gratefully acknowledges the support from the EPSRC Centre for Doctoral Training in *Integrative Sensing and Measurement*, through a Program [grant number EP/L016753/1]. This work was also funded by the UK EPSRC Quantum Technology Hub in Quantum Enhanced Imaging through a Program [grant number EP/M01326X/1]. DBP would like to thank the Royal Academy of Engineering for support.

## References

(1) Krenn, M.; Fickler, R.; Fink, M.; Handsteiner, J.; Malik, M.; Scheidl, T.; Ursin, R.; Zeilinger, A. *New J. Phys.* **2014,** *16,* 113028.
(2) Maurer, C.; Jesacher, A.; Bernet, S.; Ritsch-Marte, M. *Laser Photon. Rev.* **2011,** *5,* 81–101.
(3) D'Ambrosio, V.; Nagali, E.; Walborn, S.P.; Aolita, L.; Slussarenko, S.; Marrucci, L.; Sciarrino, F. *Nat. Commun.* **2012,** *3,* 961–969.
(4) Mafu, M.; Dudley, A.; Goyal, S.; Giovannini, D.; McLaren, M.; Padgett, M.J.; Konrad, T.; Petruccione, F.; Lütkenhaus, N.; Forbes, A. *Phys. Rev. A* **2013,** *88,* 032305–032313.
(5) Allen, L.; Beijersbergen, M.W.; Spreeuw, R.J.C.; Woerdman, J.P. *Phys. Rev. A* **1992,** *45,* 8185–8189.
(6) Yao, A.M.; Padgett, M.J. *Adv. Opt. Photonics* **2011,** *3,* 161–204.
(7) Bazhenov, V.Y.; Vasnetsov, M.; Soskin, M. *JETP Lett.* **1990,** *52,* 429–431.
(8) Swartzlander, G.A.; Hernandez-Aranda, R.I. *Phy. Rev. Lett.* **2007,** *99,* 163901.
(9) Acheson, D. *Elementary Fluid Dynamics: Oxford Applied Mathematics and Computing Science Series*; Oxford University Press: Oxford, **1990**.
(10) Maleev, I.D.; Palacios, D.M.; Marathay, A.S.; Swartzlander, G.A. Jr. *J. Opt. Soc. Am. B* **2004,** *21,* 1895–1900.

(11) Palacios, D.; Maleev, I.; Marathay, A.; Swartzlander, G Jr. *Phy. Rev. Lett.* **2004,** *92,* 143905.
(12) Palacios, D.; Rozas, D.; Swartzlander, G.A. Jr. *Phy. Rev. Lett.* **2002,** *88,* 103902.
(13) Ding, P.F.; Pu, J. *Opt. Express* **2014,** *22,* 1350–1358.
(14) Padgett, M.J.; Allen, L. *Opt. Commun.* **1995,** *121,* 36–40.
(15) Rodenburg, B.; Lavery, M.P.J.; Malik, M.; O'Sullivan, M.N.; Mirhosseini, M.; Robertson, D.J.; Padgett, M.; Boyd, R.W. *Opt. Lett.* **2012,** *37,* 3735–3737.
(16) Gibson, G.; Courtial, J.; Padgett, M.J.; Vasnetsov, M.; Pas'ko, V.; Barnett, S.M.; Franke-Arnold, S. *Opt. Express* **2004,** *12,* 5448–5456.
(17) Fürhapter, S.; Jesacher, A.; Bernet, S.; Ritsch-Marte, M. *Opt. Express* **2005,** *13,* 689–694.
(18) Aspden, R.S.; Morris, P.A.; He, R.; Chen, Q.; Padgett, M.J. *J. Opt.* **2016,** *18,* 055204.
(19) Lee, J.H.; Foo, G.; Johnson, E.G.; Swartzlander, G.A. Jr. *Phy. Rev. Lett.* **2006,** *97,* 053901.
(20) Mandel, L.; Wolf, E. *Optical Coherence and Quantum Optics*; Cambridge University Press: Cambridge, **1995**.
(21) Vasnetsov, M.; Pas'ko, V.; Soskin, M. *New J. Phys.* **2005,** *7,* 46–63.
(22) Liu, R.; Phillips, D.; Li, F.; Williams, M.; Andrews, D.; Padgett, M. *J. Opt.* **2015,** *17,* 045608.